SIMULATION OF THE IMMISCIBLE DISPLACEMENT IN POROUS MEDIA USING CAPILLARY PRESSURE AND RELATIVE PERMEABILITY CURVES FROM TRANSIENT AND STEADY-STATE EXPERIMENTS

C. D. Tsakiroglou[1,*], D.G. Avraam[3], A. C. Payatakes[1,2]
[1]FORTH / ICE-HT, Stadiou Street, Platani, P.O. Box 1414, GR – 26504 Patras, Greece
[2]Department of Chemical Engineering, University of Patras, GR – 26504 Patras, Greece
[3]Prefecture of Imathia, Sec. of Town-Planning & Environment, GR - 59100 Veria, Greece

This paper was prepared for presentation at the International Symposium of the Society of Core Analysts held in Abu Dhabi, UAE, 5-9 October 2004

ABSTRACT

The relative permeability, k_{rw}, k_{ro}, and capillary pressure, P_c, curves, are estimated with history matching from transient displacement experiments performed on a model porous medium, at varying values of the capillary number, Ca, for two fluid systems: one of intermediate and one of strong wettability. The transient k_{rw}, k_{ro} are compared to corresponding ones measured with the steady-state method on the same porous medium. Potential differences of the two-phase flow coefficients are interpreted in the light of the transient growth pattern, and the steady-state two-phase flow regimes identified at the pore network scale. The macroscopic two-phase flow equations of the transient immiscible displacement of two fluids in a 2-D porous medium are simulated with finite elements by using as input data the steady-state and transient k_{rw}, k_{ro} and ignoring or accounting for the capillary pressure term. For the same porous medium and comparable experimental conditions, the steady-state relative permeability functions may differ significantly from the corresponding transient ones, whereas both are sensitive to the capillary number and wettability.

INTRODUCTION

The effective two-phase flow coefficients of porous media, such as the capillary pressure, P_c, and relative permeability, k_{rw}, k_{ro}, functions bridge the gap between the microscopic flow dynamics and the macroscopic behavior at the reservoir scale. From this point of view, the introduction of reliable functional forms of P_c and k_{rw}, k_{ro} into the macroscopic "black" oil simulators is of key importance for the quality of numerical results that commonly are used to forecast the long-term reservoir production. Earlier experimental [20,29,30] and theoretical [1,2,7,10,12,17,20,25] studies have revealed that the transient growth pattern of the displacement of a non-wetting fluid by a wetting one

* Corresponding author, e-mail: ctsakir@iceht.forth.gr, Tel.: 2610 965212, Fax: 2610 965223

(imbibition), and vice-versa (drainage), depends on a variety of factors such as the pore space morphology, the capillary number, Ca, the viscosity ratio, κ, and wettability as it is expressed by the equilibrium contact angle, θ_e. Data of unsteady displacement experiments, such as the transient responses of the (i) fluid volumes produced, (ii) pressure drop across the porous medium, and (iii) axial distribution of the fluid saturation are fitted either explicitly [18] or implicitly [19,21,23,24,26-28] (history matching) to the macroscopic two-phase flow equations [22,31] to estimate the P_c and k_{rw}, k_{ro}. There is strong evidence that the so-estimated relative permeability and capillary pressure curves are correlated strongly with capillary number and viscosity ratio [6,8,13-15,17,24,27,28]. Such correlations have occasionally been attributed to the interactive effects of the various local forces (e.g. capillary, viscous, gravity, etc) on the displacement growth pattern at the pore network scale [2,8,10,15,17,28]. In addition to the transient techniques, steady-state core analysis tests are often employed to determine the P_c, k_{rw}, k_{ro} [3-5,9,11]. A systematic parametric analysis of the experiments of the simultaneous flow of two phases through a glass-etched chamber-and-throat network of well-characterized topology and geometry [3,5], allowed the identification of several two-phase flow regimes dominating over different ranges of the parameter space $(S_w, Ca, \kappa, \theta_e)$. Accordingly, the steady-state relative permeability functions were found to change strongly with Ca, κ, θ_e [3,5] whereas the existence of non-linear viscous coupling effects on k_{rw}, k_{ro} suggested the use of the generalized rather than the conventional formulation of relative permeabilities [4,5].

In spite of the knowledge that has been accumulated from earlier studies, there is still an ambiguity concerning the adequacy of P_c, k_{rw}, k_{ro} which are fed as input parametric equations into the simulators of the transient immiscible displacement of two fluids in porous media. Unavoidably, some fundamental questions of reservoir engineering are still unanswered: (a) how dependable are the results we get by using steady-state k_{rw}, k_{rnw} curves in transient numerical simulators? (b) how large an error is introduced in the macroscopic numerical predictions, if the dependence of P_c, k_{rw}, k_{rnw} on the flow rates and viscosity ratio is ignored? (c) which is the most efficient strategy for the determination of the P_c, k_{rw}, k_{rnw} functions for a macro-scale simulator?

In the present work, transient imbibition experiments are performed, at varying Ca values, on the porous medium model used in steady-state studies [3,5] by using two fluid systems, one of intermediate and one of strong wettability. The post-breakthrough transient responses of the total wetting phase saturation and pressure drop across the porous medium are measured and introduced into a 1-D history matching algorithm to estimate simultaneously the $P_c(S_w)$ and $k_{rw}(S_w), k_{ro}(S_w)$ as functions of Ca. The estimated $k_{rw}(S_w), k_{ro}(S_w)$ are compared to the corresponding steady-state results, and potential differences are interpreted in light of the mechanisms governing the two processes.

METHODS AND MATERIALS

The porous medium model is a chamber-and-throat planar network (Fig.1a) fabricated by a photo-etching technique [3, 30], and being identical to that used in steady-state two-phase flow experiments [3-5]. Each end of the pore network is extended with triangular segments which serve as flow distributors and eliminate the end effects (Fig.1b). Holes drilled at the ends of flow distributors serve as inlet and outlet ports. The dimensions of the main pore network is (length x width) 0.16m x 0.11m, and the distance between the centers of adjacent chambers (length of periodicity) is $1221\,\mu m$. More details about the features of the glass micromodel can be found in [3].

Details of the experimental procedure (Fig.1b) that is commonly followed in an unsteady-state experiment are reported in [28-30]. Two fluid systems of intermediate (1) and strong (2) wettability were used (Table 1). Initially, the porous medium was fully occupied by the non-wetting phase (oil - o). By using a syringe pump, the wetting phase (water - w) was injected in the pore network at constant influx rate through the inlet ports. All experiments were carried out under controlled values of the capillary number Ca and viscosity ratio κ defined by

$$Ca = \mu_w u_t / \gamma_{ow} \qquad \text{and} \qquad \kappa = \mu_o / \mu_w \tag{1}$$

respectively, where u_t is the superficial flow velocity of the injected wetting phase at the entrance, μ_w is the viscosity of the wetting phase, γ_{ow} is the o/w interfacial tension, and μ_o is the viscosity of the non-wetting phase. Snap-shots of the displacement (Fig.2) were captured by a CCD camera equipped with magnification lenses. The absolute pressure of the wetting phase at the inlet tubes was measured continuously with the aid of three pressure transducers connected to a pressure converter (Fig.1b). After the end of each experiment, the actual pressure drop across the entire pore network was calculated by subtracting the pressure drops due to the viscous flow along the injection/ extraction tubes and hydrostatic heights, and averaging the measurements of the three transducers (Fig.1b). Before the breakthrough of the wetting phase, its saturation varies linearly with time, and for this reason the pre-breakthrough saturation data were ignored in the analysis. After the breakthrough, the transient variation of S_w was measured precisely by collecting the fluids expelling from the pore network, in a calibrated glass capillary tube. The accuracy of this measurement was improved by video-recording the position of the meniscus separating the two fluids collected in the capillary tube (Fig.1b).

RELATIVE PERMEABILITIES AND CAPILLARY PRESSURES

History matching

The immiscible displacement of oil (o) by water (w) in a homogeneous and isotropic porous medium is described by the conventional mass and momentum balances for each phase [24], namely

$$\phi\frac{\partial S_o}{\partial t}+\frac{\partial u_o}{\partial x}=0 \tag{2}$$

$$\varphi\frac{\partial S_w}{\partial t}+\frac{\partial u_w}{\partial x}=0 \tag{3}$$

$$u_w=\frac{kk_{rw}}{\mu_w}\left(-\frac{\partial P_w}{\partial x}\right) \tag{4}$$

$$u_o=\frac{kk_{ro}}{\mu_o}\left(-\frac{\partial P_o}{\partial x}\right) \tag{5}$$

In the foregoing equations, u_i, S_i, P_i, k_{ri} are the local values of the superficial flow velocity, saturation, pressure and relative permeability of phase $i(=w,o)$, respectively, and k is the absolute permeability of the porous medium. The capillary pressure is defined as the difference between the local pressures of the two fluids and is written as

$$P_c=P_o-P_w \tag{6}$$

whereas the fluid saturations are interrelated by

$$S_w+S_o=1.0 \tag{7}$$

By substituting the fluid flow velocity, u_w, with the fractional flow, F_w, defined by

$$F_w=\frac{u_w}{u_t} \qquad 0\le F_w\le 1.0 \tag{8}$$

and using the dimensionless variables

$$\xi=\frac{x}{L} \quad \text{and} \quad \tau=\frac{u_t t}{\phi L} \tag{9}$$

Eqs.(2)-(5) are transformed to

$$\frac{\partial S_w}{\partial \tau}+\frac{\partial F_w}{\partial \xi}=0 \tag{10}$$

$$F_w=1-\frac{k_{ro}}{k_{ro}+\kappa k_{rw}}\left[1-\frac{u_c}{u_0}k_{rw}\frac{\partial P_c^*}{\partial S_w}\frac{\partial S_w}{\partial \xi}\right] \tag{11}$$

$$\left(-\frac{\partial P_w^*}{\partial \xi}\right)=\frac{\kappa}{k_{ro}+\kappa k_{rw}}\left[\frac{u_0}{u_c}+\frac{k_{ro}}{\kappa}\frac{\partial P_c^*}{\partial S_w}\frac{\partial S_w}{\partial \xi}\right] \tag{12}$$

(13)

where the dimensionless variables P_c^* and P_w^* are defined by

$$P_c^*=\frac{P_c}{\Delta P_w^0} \qquad P_w^*=\frac{P_w}{\Delta P_w^0} \tag{14}$$

the characteristic velocity u_c is given by

$$u_c=\frac{k\Delta P_w^0}{\mu_w L} \tag{15}$$

and ΔP_w^0 is the steady-state pressure drop across the porous medium for $S_w = 1$ and $k_{rw} = 1$. By regarding the pore network ($0 \le \xi \le 1$) as a part of a semi-infinite porous medium, and ignoring capillary end effects in waterflood [16,19,21,24], Eqs.(10) and (11) are subject to the initial condition

$$S_w(0,\xi) = 0 \tag{16}$$

left boundary condition

$$S_w(\xi = 0) = 1 - S_{or} \tag{17}$$

and right boundary condition

$$\left(\frac{\partial S_w}{\partial \xi}\right)_{\xi=\xi_0} = 0 \tag{18}$$

where ξ_0 is set equal to 10. The pressure gradient $\left(-\partial P_w^* / \partial \xi\right)$ is an explicit function of S_w and is post-calculated from the numerical solution of the PDE [28]. With respect to the dimensionless saturation

$$S_w^* = \frac{S_w}{1 - S_{or}} \tag{19}$$

the capillary pressure and relative permeability curves may be given by the following functional forms [23,27,28]

$$P_c = P_c^0 \left(S_w^* + h\right)^{-m_c} \tag{20}$$

$$k_{rw} = k_{rw}^0 \frac{\left(S_w^* + h_w\right)^{m_w} + a_w S_w^*}{\left(1 + h_w\right)^{m_w} + a_w} \tag{21}$$

$$k_{ro} = k_{ro}^0 \frac{\left(1 - S_w^* + h_o\right)^{m_o} + a_o\left(1 - S_w^*\right)}{\left(1 + h_o\right)^{m_o} + a_o} \tag{22}$$

The parameters $P_c^0, k_{rw}^0, m_c, m_w, m_o, a_w, a_o$ are estimated with history matching, while it is assumed that $h_w = h_o = 10^{-4}$ and $k_{ro}^0 = 1$. The residual oil saturation, S_{or}, was set equal to the experimentally measured value. History matching was done in the environment of the commercial software package ATHENA by using finite differences and the method of lines to integrate the PDE, and Bayesian estimation to fit the numerical results to the experimental datasets [28]. The numerically calculated values of $S_w(\tau, \xi)$ and $\left(-\partial P_w^* / \partial \xi\right)_{\tau,\xi}$ were integrated along the entire length of the porous medium for the determination of the total water saturation, $S_{wt}(\tau)$, and the total pressure drop across the wetting fluid, $\Delta P_{wt}(\tau)$.

Steady-state relative permeability and capillary pressure functions

The steady-state relative permeability functions have been determined during the simultaneous flow of both fluids through the same porous medium by measuring the pressure drop across each phase and the time averaged water saturation within the central area of the network with image analysis [3]. Taking into account the theoretical end values $k_{rw}(S_w = 0) = 0$, $k_{r0}(S_w = 1 - S_{or}) = 0$, $k_{r0}(S_w = 0) = 1$, the conventional steady-state relative permeability curves were fitted (Fig.3b) with 3-parameter sigmoid functions of the form

$$k_{rw} = b_w \exp\left[-\exp\left(-g_w\left(S_w - S_{cw}\right)\right)\right] - b_w \exp\left[-\exp\left(g_w S_{cw}\right)\right] \tag{25}$$

$$k_{ro} = b_o \exp\left[-\exp\left(-g_o\left(1 - S_w - S_{co}\right)\right)\right] + AS_w + B \tag{26}$$

where

$$B = 1 - b_o \exp\left[-\exp\left(-g_o\left(1 - S_{co}\right)\right)\right] \tag{27}$$

$$A = \left\{-b_o \exp\left[-\exp\left(-g_o\left(S_{or} - S_{co}\right)\right)\right] - B\right\}/\left(1 - S_{or}\right) \tag{28}$$

The experimental measurements [3] indicated a relatively small gradient of the capillary pressure across the porous medium (the term $\Delta P_c/\Delta\xi$ was small but finite), which was attributed to capillary end effects [16, 26]. Such data along with the axial distribution of the time averaged water saturation across a well-defined area of the pore network could be fitted to an integral equation resulting from Darcy law [16] in order to estimate the capillary pressure curve.

SIMULATION OF THE DISPLACEMENT IN 2-D POROUS MEDIA

The immiscible displacement of two fluids in a 2-D porous medium is described by the following dimensionless equations [19,21]

$$\left(1 - S_{or}\right)\frac{\partial S_w^*}{\partial \tau} - \nabla^* \cdot \left(\frac{u_c}{u_0} k_{rw} \nabla^* P_w^*\right) = 0 \tag{23}$$

$$\nabla^* \cdot \left[\left(k_{rw} + \frac{k_{ro}}{\kappa}\right)\nabla^* P_w^* + \left(1 - S_{or}\right)\frac{k_{ro}}{\kappa}\frac{\partial P_c^*}{\partial S_w^*}\nabla^* S_w^*\right] = 0 \tag{24}$$

The foregoing equations are solved by using finite elements with triangular Galerkin approximations in the environment of the commercial software Flex-PDE 3. The accurate geometry of the experimental model is transformed to a numerical grid, and realistic boundary conditions are used: (i) the fluxes of pressure and saturation are set equal to zero on the solid wall surrounding the pore network; (ii) the outlet pressure is kept equal

to atmosphere; (iii) the pressure fluxes at the inlet ports are given by Darcy law; (iv) the water saturation at the inlet ports is set equal to $1-S_{or}$.

RESULTS AND DISCUSSION

For the case of intermediate wettability, the $k_{rw}(S_w), k_{ro}(S_w)$ estimated from transient displacements are shown in Fig.3a. In transient imbibition experiments under unfavorable viscosity ratio ($\kappa > 1$), and intermediate wettability, the growth pattern is governed by three competitive mechanisms depending on Ca [20,22,29,30]: (i) viscous fingering is favored by high Ca values; (ii) capillary fingering with a compact rather than an invasion percolation front is favored by low Ca values; (iii) frontal displacement is favored by high Ca values. The sweep efficiency and hence $k_{rw}(S_w)$ increase as frontal displacement is dominant and decreases when either viscous fingering or capillary fingering prevails. In this manner, the $k_{rw}(S_w)$ estimated at Ca=10^{-6} is slightly greater than that estimated at Ca=5x10^{-6} (Fig.3a) as the flow pattern is a mixture of frontal displacement and viscous fingering (Fig.2). However, a dramatic decrease of $k_{rw}(S_w)$ occurs at Ca=10^{-7} (Fig.3a) where the capillary fingering becomes evident. On the other hand, the $k_{ro}(S_w)$ has a tendency to increase at decreasing Ca values. This might be attributed to the compact nature of the displacement pattern and the preservation of the continuity of oil at least at low water saturations (Fig.3a).

In steady-state imbibition experiments performed under a constant Ca value, the transition from one S_w value to another is carried out by varying the flow rate ratio q_o/q_w [3,5]. Unavoidably, the two-phase flow regime varies not only with Ca but also with S_w. In general, the steady-state $k_{rw}(S_w), k_{ro}(S_w)$ are increasing functions of Ca (Fig.3b) as the flow regime progressively changes from large-ganglion dynamics (LGD) to small-ganglion dynamics (SGD) to drop traffic flow (DTF) and to connected flow pathways (CPF) [3,5]. The mobility of oil increases because of the motion of small ganglia populations (SGD) and oil droplets (DTF), whereas the mobility of water increases as the populations of moving large ganglia, reducing the number of free flow paths, decreases and stranded small ganglia are remobilized [3] (Fig.3b).

For the case of intermediate wettability, the transient $k_{rw}(S_w)$ is always greater than the steady-state $k_{rw}(S_w)$; it tends to coincide with it at high Ca values, whereas both are linear functions of S_w (Fig.4a-c). The steady-state $k_{ro}(S_w)$ is greater or lower than the transient one at high or low Ca values, respectively (Fig.4a-c). Such a different behavior can be explained with reference to the ratio of moving to stranded ganglia. This ratio is a strongly increasing function of Ca, and may take on very high values in steady-state experiments, while it is less sensitive to Ca and takes on relatively low values in transient experiments. The $P_c(S_w)$ estimated from transient imbibition data is a decreasing

function of Ca (Fig.4d) in agreement with the linear thermodynamic theory of Hassanizadeh et al [15].

In the case of strong wettability and steady-state experiments [5], the presence of thin wetting films along the pore walls results in disconnection of oil to a large extent in the form of ganglia and droplets. The high $k_{ro}(S_w)$ values are due to the mobilization of the small ganglia (SGD) and droplets (DTF) and the lubricating effect of the thin wetting films surrounding the viscous oil (Fig.5a,b). In transient experiments performed at relatively low Ca values, the advancement of precursor wetting films along pore wall microroughness [31,32] and the consequent snap-off in throats are the main reasons for the entrapment of oil ganglia in the pore network, and the sharp decrease of the $k_{ro}(S_w)$ at low water saturations (Fig.5b).

CONCLUSIONS

The relative permeability and capillary pressure functions determined from transient displacement (history matching) and steady-state two-phase flow experiments, all performed on a well-characterized glass-etched pore network, are analyzed. The two-phase flow coefficients determined by both methods are sensitive to the capillary number and wettability, in accordance with the transient displacement growth pattern and steady-state two-phase flow regimes identified at the network scale. Unavoidably, very different simulated results of the immiscible displacement in porous media may be obtained by using the steady-state or transient relative permeability curves, and ignoring or including the capillary pressure terms.

REFERENCES

1. Aker, E., and K.J. Maloy, “Simulating temporal evolution of pressure in two-phase flow in porous media”, *Phys Rev. E* (1998) **58**, 2217-2226.
2. Aker, E, K.J. Maloy, A. Hansen, and G.G. Batrouni, “A two-dimensional network simulator for two-phase flow in porous media”, *Transp. Porous Media* (1998) **32**, 163-186.
3. Avraam, D.G. and A.C. Payatakes, “Flow regimes and relative permeabilities during steady-state two-phase flow in porous media” *J. Fluid Mech.*, (1995) **293**, 207-236.
4. Avraam, D.G. and A.C. Payatakes, “Generalized relative permeability coefficients during steady-state two-phase flow in porous media and correlation with the flow mechanisms. *Transp. Porous Media* (1995) **20**, 135-168.
5. Avraam, D.G. and A.C. Payatakes, “Flow mechanisms, relative permeabilities, and coupling effects in steady-state two-phase flow through porous media. The case of strong wettability”, *Ind. Eng. Chem. Res.* (1999) **38**, 778-786.
6. Beliaev, A.Y. and S.M. Hassanizadeh, “A theoretical model of hysteresis and dynamic effects in the capillary relation for two-phase flow in porous media”, *Transp. Porous Media* (2001) **43,** 487-510.
7. Blunt M. and P. King, “Relative permeabilities from two- and three-dimensional pore-scale network modeling”, *Transp. Porous Media*, (1991) **6**, 407-?

8. Constantinides, G.N. and A.C. Payatakes, "Determination of the effects of capillary number, viscosity ratio and wettability on the capillary pressure-saturation relation using an advanced pore network simulator", SPE Paper No 78518, presented at the 10th Abu-Dhabi International Petr. Exhib and Confer., Abu-Dhabi, Oct. 13-16, 2002.
9. Constantinides, G.N. and A.C. Payatakes, "Network simulation of steady-state two-phase flow in consolidated porous media", *AIChE J.*, (1996) **42**, 369-382.
10. Constantinides, G.N. and A.C. Payatakes, "Effects pf precursor wetting films in immiscible displacement through porous media", *Transp. Porous Media*, (2000) **38**, 291-317.
11. Fourar, M., S. Bories, R. Lenormand, and P. Persoff, "Two-phase flow in smooth and rough fractures: measurement and correlation by porous-medium and pipe flow models" *Water Resour. Res.*, (1993) **29**, 3699-3708.
12. Goode P.A. and T.S. Ramakrishnan, "Momentum transfer across fluid-fluid interfaces in porous media: a network model", *AIChE J.*, (1993) **39**,1124-1134.
13. Hassanizadeh, S.M. and W.G. Gray, "Thermodynamic basis of capillary pressure in porous media", *Water Resour. Res.*, (1993) **29**, 3389-3405.
14. Hassanizadeh, S.M. and W.G. Gray, "Toward an improved description of the physics of two-phase flow", *Adv. Water Resour.*, (1993) **16**, 53-67.
15. Hassanissadeh, S.M., M.A. Celia and H.K. Dahle, "Dynamic effect in the capillary pressure- saturation relationship and its impacts on unsaturated flow", *Vadoze Zone J.*, (2002) **1**, 38-57.
16. Huang, D.D. and M.M. Honarpour, "Capillary end effects in coreflood calculations", *J. Pet. Sci. Eng.*, (1998) **19**, 103-117.
17. Hughes R.G. and M.J. Blunt, "Pore scale modeling of rate effects in imbibition" *Transp. Porous Media*, (2000) **40**, 295-322.
18. Johnson, E.F., D.P. Bossler and V.O. Naumann, "Calculation of relative permeability from displacement experiments", *J. Pet. Tech.*, (1959) **January**, 61-63.
19. Kulkarni, R., A.T. Watson, J.-E. Norttvedt and A. Sylte, "Two-phase flow in porous media: property identification and model validation", *AIChE J.*, (1998) **44**, 2337-2350.
20. Lenormand, R., E. Touboul, and C. Zarcone, "Numerical models and experiments on immiscible displacement in porous media", *J. Fluid Mech.*, (1988) **189**, 165-187.
21. Mejia, G.M., K.K. Mohanty and A.T. Watson, "Use of in situ saturation data in estimation of two-phase flow functions in porous media", *J. Pet. Sci. Eng.*, (1995) **12**, 233-245.
22. Sahimi M., *Flow and Transport in Porous Media and Fractured Rock**:** From Classical Methods to Modern Approaches*, VCH, Weinheim, Germany (1995).
23. Sigmund, P. and F. McCaffery, "An improved unsteady-state procedure for determining the relative permeability characteristics of heterogeneous media", *SPE J.*, (1979) **169**, 15-28.
24. Singh, M., V. Mani, M.M. Honarpour and K.K. Mohanty, "Comparison of viscous and gravity dominated gas-oil relative permeabilities", *J. Pet. Sci. Eng.*, (2001) **30**, 67-81.

25. Singh, M. and K.K. Mohanty, "Dynamic modelling of drainage through three-dimensional porous materials", *Chem. Eng. Sci.*, (2003) **58**, 1-18.
26. Toth, J., T. Bodi, P. Szucs and F. Civan, "Convenient formulae for determination of relative permeability from unsteady-state fluid displacements in core plugs", *J. Pet. Sci. Eng.*, (2002) **36**, 33-44.
27. Tsakiroglou, C.D., "Correlation of the two-phase flow coefficients of porous media with the rheology of shear-thinning fluids", *J. Non-Newtonian Fluid Mech.*, (2004) **117**, 1-23.
28. Tsakiroglou, C.D., M. Theodoropoulou, and V. Karoutsos, "Non-equilibrium capillary pressure and relative permeability curves of porous media", *AIChE J.*, (2003) **49**, 2472-2486.
29. Tzimas, G.C., T. Matsuura, D.G. Avraam, W. van der Brugghen, G.N. Constantinides, and A.C. Payatakes, "The combined effect of the viscosity ratio and the wettability during forced imbibition through nonplanar porous media", *J. Colloid Interface Sci.* (1997) **189**, 27-36.
30. Vizika, O., D.G. Avraam, and A.C. Payatakes, "On the role of the viscosity ratio during low-capillary number forced imbibition in porous media", *J. Colloid Interface Sci.*, (1994) **165**, 386-401.
31. Whitaker, S., "Flow in porous media II: The governing equations for immiscible, two-phase flow", *Transp. Porous Media*, (1986) **1**, 105-125.

Table 1. Physicochemical properties of fluid systems

	System 1	System 2
Non-wetting fluid (oil, o)	n-hexadecane	n-nonanol
Wetting fluid (water, w)	Distilled water	Formamide
Oil viscosity, μ_o (Pa s)	0.00315	0.00964
Water viscosity, μ_w (Pa s)	0.00094	0.000335
Oil density, ρ_o (Kg/m^3)	774	816
Water density, ρ_w (Kg/m^3)	995	1116
Interfacial tension, γ (mN/m)	25	4.3
Equilibrium contact angle, θ_e (^{o})	42	9

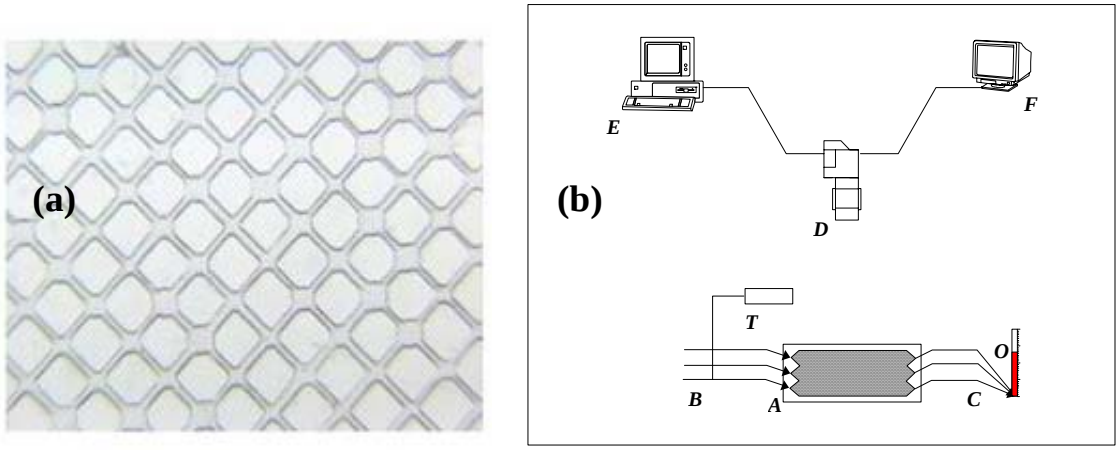

Figure 1. (a) A segment of the glass-etched chamber-and-throat network used in experiments (the distance between the centres of two adjacent chambers is 1220 μm). (b) Experimental apparatus: A=porous medium model; B=fluid injection tubes; C=fluid withdrawal tubes; D=CCD video-camera; E=computer; F=monitor; T=absolute pressure converter; O=calibrated capillary tube for the measurement of the volume of fluids expelling from the porous medium.

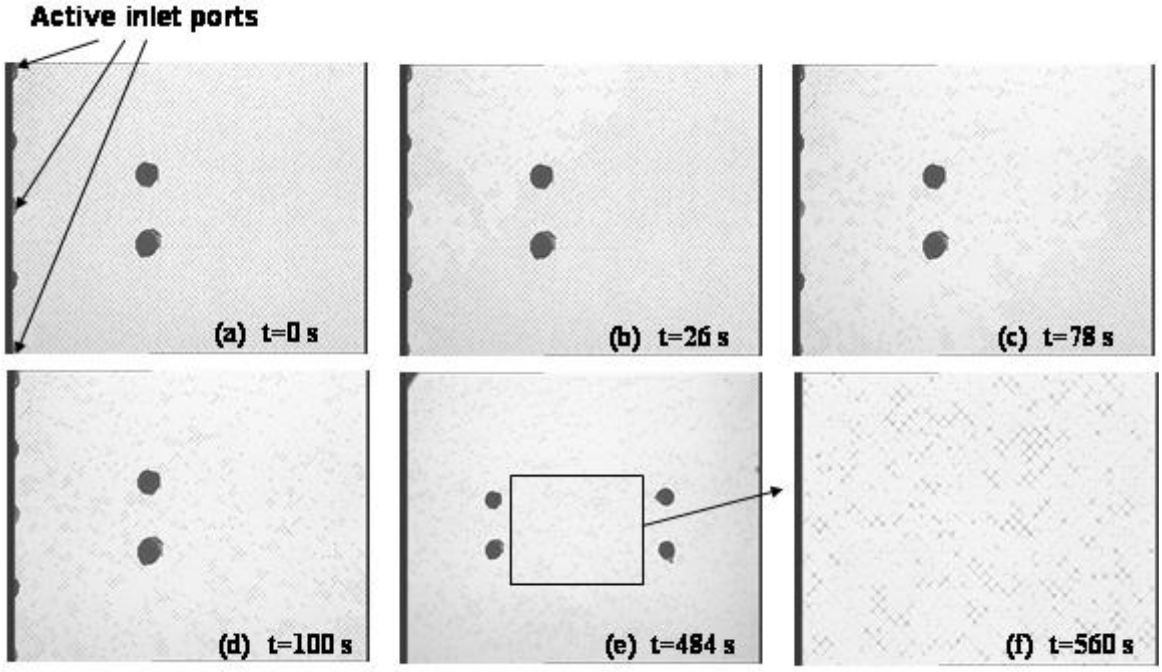

Figure 2. (a-d) Successive snap-shots of the immiscible displacement of n-hexadecane (dark phase) by distilled water (white phase) at $Ca=1.19x10^{-6}$. (e) Spatial fluid distribution in the pore network after long time (steady-state). (f) Magnification of the central zone of the pore network (the black spots are trapped oil ganglia).

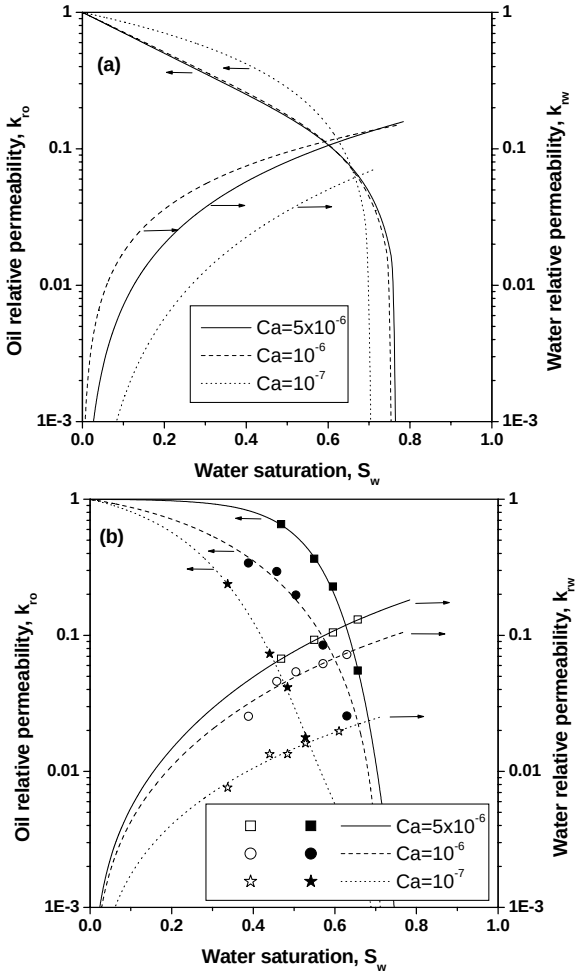

Figure 3. (a) Estimated transient relative permeability functions of Eqs.(21) and (22) for the system n-hexadecane/distilled water. (b) Experimentally measured steady-state relative permeabilities (symbols) fitted with the sigmoid functions of Eqs.(25)-(28) (lines), for the system n-hexadecane/distilled water.

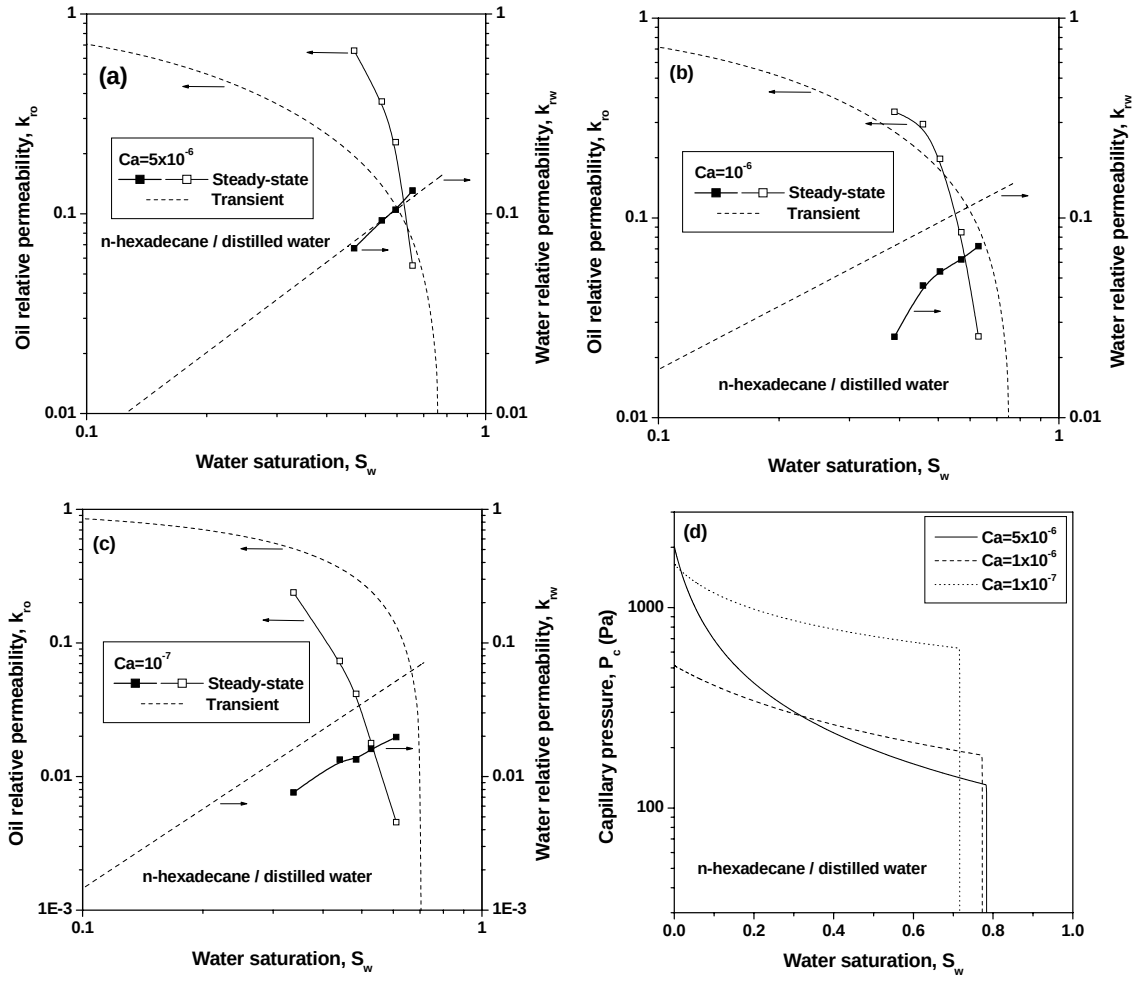

Figure 4. (a-c) Comparison of measured steady-state with (history matching) estimated transient relative permeability curves for the fluid system of intermediate wettability. (d) Capillary pressure curves estimated from transient experiments at various Ca values.

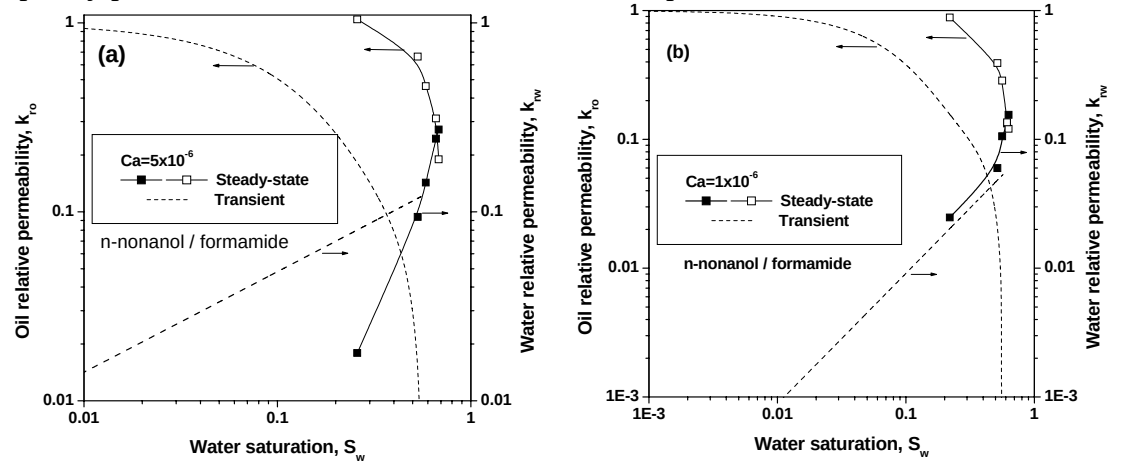

Figure 5. Comparison of measured steady-state with (history matching) estimated transient relative permeability curves for the fluid system of strong wettability.